JOURNAL OF AIRCRAFT
Vol. 37, No. 4, July–August 2000

Hypersonic Flow Predictions Using Linear and Nonlinear Turbulence Closures

U. Goldberg,* P. Batten,† S. Palaniswamy,* S. Chakravarthy,‡ and O. Peroomian†
Metacomp Technologies, Inc., Westlake Village, California 91361

Two- and three-dimensional hypersonic flow cases are computed using linear one-equation closures and a nonlinear two-equation model, where the anisotropy tensor is modeled as a cubic function of mean strain and vorticity tensors. The latter is found to excel in predicting bypass transition, whereas the one-equation R_t model is very good at heat-transfer prediction. Both closures excel in predicting pressure distributions; however, the nonlinear model is found to overpredict heat-transfer. This suggests that in separated flow regions with simultaneously low mean-flow kinetic energy (and therefore low strain magnitude) and high temperature gradients, overpredicted levels of turbulence length scale can lead to rather small errors in the turbulent shear stress, while at the same time leading to a large overprediction of the turbulent heat fluxes. The simpler one-equation R_t model is therefore a good candidate for engineering prediction of hypersonic heat-transfer.

I. Introduction

THERE has recently been renewed interest in hypersonic flight vehicles. Projects such as Sandia laboratories' Hypersoar and Boeing's Hyper-X are current examples. The engine inlets of such vehicles typically involve compression ramps, which, through a series of shocks, reduce the engine inflow velocity to enable more efficient combustion. Such a shock system imposes a severe penalty in terms of surface heating, requiring careful attention to the choice of materials and/or cooling devices to avoid the possibility of local ablation of the vehicle's skin. It is important, therefore, to be able to predict hypersonic flow over ramp/wedge configurations, including surface heating characteristics, with the aim of using this capability for analysis and design of vehicle components such as engine inlets. The ability to predict turbulent hypersonic flows with a high level of confidence carries much broader benefits for entire vehicle external/internal flow prediction and design capability.

Conventional linear k–ϵ models are notorious for severely overpredicting heat-transfer levels in flows involving strong enough adverse pressure gradient to cause separation, as documented in detail by Launder.[1] This stems from ill-understood defficiencies in the ϵ transport equation in nonequilibrium near-wall regions, which can lead to excessive levels of the length scale generated in separated flows and hence to correspondingly excessive heat-transfer levels, especially in the reattachment region. The k–ϵ closure applied in this work does include a nonequilibrium modification to the ϵ equation, but this is evidently not powerful enough to overcome the near-wall length scale problem. It is, therefore, desirable to evaluate the performance of single-equation closures in predicting flows involving heat-transfer under strong nonequilibrium conditions. This paper tests the capability of three such turbulence closures to predict heat-transfer under hypersonic flow conditions: the R_t model,[2] the Spalart–Allmaras (S–A) model,[3] and Menter's model.[4] The formulation of the latter two models is given in detail in Refs. 3 and 4, respectively, and the R_t model is described next. Based on the results of a Mach 9 ramp flow,[5] the latter closure was used to predict a three-dimensional Mach 8 inlet flow. The cubic k–ϵ model, however, is better equipped to predict bypass transition than either its base (linear) model or the R_t model is, as demonstrated on a Mach 8 transitional flow test case.

Received 17 October 1999; revision received 7 February 2000; accepted for publication 28 February 2000.

*Senior Scientist, 650 Hampshire Road, No. 200.
†Scientist, 650 Hampshire Road, No. 200.
‡President and Chief Scientist, 650 Hampshire Road, No. 200.

II. Formulation of Turbulence Models

A. Cubic k–ϵ Model

This nonlinear model[6] accounts for both Reynolds-stress anisotropy and streamline curvature, including swirl effects. The Reynolds stresses are modeled using the mean strain and vorticity relations from the quadratic model of Shih et al.[7] with the cubic extension proposed by Lien and Leschziner.[8]

Following the notation of Loyau et al.,[9] Cartesian tensors of rank 2 are denoted by bold, nonitalic symbols ($\boldsymbol{a}, \boldsymbol{b}$, etc.), with the following conventions:

$$\boldsymbol{a} = a_{ij}, \qquad \boldsymbol{ab} = a_{ik}b_{kj}, \qquad \boldsymbol{abc} = a_{ik}b_{kl}c_{lj}, \text{ etc.}$$

$$\boldsymbol{a}^2 = a_{ik}a_{kj}, \qquad \{\boldsymbol{a}^2\} = a_{ik}a_{ki}, \qquad \boldsymbol{I} = \delta_{ij}$$

The canonical form of a cubic model is then written as

$$\begin{aligned}\boldsymbol{a} = {} & -2C_\mu^* f_\mu \boldsymbol{S} + a_1\left(\boldsymbol{S}^2 - \tfrac{1}{3}\{\boldsymbol{S}^2\}\boldsymbol{I}\right) + a_2(\boldsymbol{WS} - \boldsymbol{SW}) \\ & + a_3\left(\boldsymbol{W}^2 - \tfrac{1}{3}\{\boldsymbol{W}^2\}\boldsymbol{I}\right) + \left(b_1\{\boldsymbol{S}^2\} + b_2\{\boldsymbol{W}^2\}\right)\boldsymbol{S} \\ & + b_3\left(\boldsymbol{W}^2\boldsymbol{S} + \boldsymbol{SW}^2 - \tfrac{2}{3}\{\boldsymbol{SW}^2\}\boldsymbol{I}\right) + b_4(\boldsymbol{WS}^2 - \boldsymbol{S}^2\boldsymbol{W}) \end{aligned} \tag{1}$$

where the nondimensional strain, vorticity, and anisotropy tensors are

$$S_{ij} = (k/2\epsilon)\left(U_{i,j} + U_{j,i} - \tfrac{2}{3}U_{k,k}\delta_{ij}\right)$$

$$W_{ij} = (k/2\epsilon)(U_{i,j} - U_{j,i}) \tag{2}$$

$$a_{ij} = \widetilde{u_i u_j}/k - \tfrac{2}{3}\delta_{ij} \tag{3}$$

The Shih et al. and Lien–Leschziner models set the coefficients in the preceding formulation as given here: a_1, $3f_\mu/(1000 + S^3)$; a_2, $15f_\mu/(1000 + S^3)$; a_3, $-19f_\mu/(1000 + S^3)$; b_1, $-16(C_\mu^*)^3 f_\mu$; b_2, $-16(C_\mu^*)^3 f_\mu$; b_3, 0; b_4, $80(C_\mu^*)^3 f_\mu$. Here

$$C_\mu^* = \tfrac{2}{3}\Big/(1.25 + S + 0.9\Omega) \tag{4}$$

$$S = \sqrt{2S_{ij}S_{ij}}, \qquad \Omega = \sqrt{2W_{ij}W_{ij}} \tag{5}$$

and the low Reynolds damping of the linear (base) model[10] is used:

$$f_\mu = \frac{1 - e^{-0.01R_t}}{1 - e^{-\sqrt{R_t}}} \max\left\{1, \left(\frac{2}{R_t}\right)^{\frac{1}{2}}\right\} \tag{6}$$

$R_t \equiv k^2/(\nu\epsilon)$ being the turbulence Reynolds number.

The exact production term $P_k = -\rho\widetilde{u_i u_j}U_{i,j}$ in which $\widetilde{u_i u_j}$ is derived from Eq. (3), is used in the k and ϵ transport equations. The base (linear) model, supplying k and ϵ in the preceding formulation,

is given in detail in Ref. 10. This topography-parameter-free model is designed for enhanced handling of flows involving adverse pressure gradient (a feature not common to k–ϵ models) using an extra source term in the ϵ transport equation. It also enforces timescale realizability by ensuring that the turbulence timescale never falls below the Kolmogorov microscale $(\nu/\epsilon)^{1/2}$.

B. Linear Single-Equation Model

The R_t model consists of solving the following transport equation for the undamped eddy viscosity R:

$$\rho\frac{\mathrm{D}R}{\mathrm{D}t}=\frac{\partial}{\partial x_j}\left[\left(\mu+\frac{\mu_t}{\sigma_R}\right)\frac{\partial R}{\partial x_j}\right]+C_1\rho(RP_k)^{\frac{1}{2}}-(C_3f_3-C_2)\rho\mathcal{D} \tag{7}$$

where D/Dt is the compressive material derivative. The turbulence production is expressed in terms of the Boussinesq model

$$P_k=\nu_t\left[\left(\frac{\partial U_i}{\partial x_j}+\frac{\partial U_j}{\partial x_i}\right)\frac{\partial U_i}{\partial x_j}-\frac{2}{3}\left(\frac{\partial U_k}{\partial x_k}\right)^2\right] \tag{8}$$

and in the destruction term

$$\mathcal{D}=\begin{cases}\dfrac{\partial R}{\partial x_j}\dfrac{\partial R}{\partial x_j}, & \varphi>0\\ 0, & \text{otherwise}\end{cases} \tag{9}$$

where

$$\varphi=\frac{\partial Q}{\partial x_j}\frac{\partial R}{\partial x_j} \tag{10}$$

and

$$Q=\left[\left(U_i-U_i^0\right)^2\right]^{\frac{1}{2}} \tag{11}$$

Here U_i^0 is the velocity vector of the frame of reference (often $\mathbf{0}$); U_i are the Cartesian velocity components; $x_i\equiv(x, y, z)$ are the corresponding coordinates; μ and μ_t are the dynamic molecular and eddy viscosities, respectively; ρ is density; and ν_t is the kinematic eddy viscosity μ_t/ρ. $\mathcal{D}$ vanishes at the location of maximum R because $\nabla R=0$ there. The conditional application retains $\mathcal{D}=0$ from that location inward.

The eddy viscosity field is given by

$$\mu_t=f_\mu\rho R \tag{12}$$

where

$$f_\mu=\frac{[\tanh(\alpha\chi^2)]}{[\tanh(\beta\chi^2)]} \tag{13}$$

and

$$\chi\equiv\rho R/\mu \tag{14}$$

The model constants and the damping function f_3 are derived from asymptotic arguments at walls and limit flow regions such as the logarithmic overlap and pipe centerline. Details are given in Refs. 2 and 11. The final results are as follows:

$$f_3=1+2\alpha/(3\beta C_3\chi) \tag{15}$$

$$C_1=\kappa^2\left(C_3-C_2-\sigma_R^{-1}\right) \tag{16}$$

$$C_2=-5\alpha/(3\beta\sigma_R) \tag{17}$$

and

$$C_3-C_2=3/(2\sigma_R) \tag{18}$$

where $\kappa=0.41$, $\sigma_R=0.8$, $\alpha=0.07$, and $\beta=0.2$.

Equation (7) is subject to the following boundary conditions:

1) Solid walls

$$R=0 \tag{19}$$

2) Freestream inflow and initial conditions:

$$R_\infty\le\nu_\infty \tag{20}$$

III. Highlights of the Numerical Approach

CFD++, a Navier–Stokes flow solver for either compressible or incompressible fluid flows, was used here. This code features a second order total variation diminishing discretization based on a multidimensional interpolation framework. For the results presented here, a Harten, Lax, van Leer, with contact wave (HLLC) Riemann solver was used to define the (limited) upwind fluxes. This Riemann solver is particularly suitable for hypersonic flow applications because, unlike classical linear solvers such as Roe's scheme, it automatically enforces entropy and positivity conditions. Further details on the numerical methodology in CFD++ can be found in Refs. 12–15.

IV. Computational Results

A. Hypersonic Flow Case 1

This example concerns flow over a curved compression surface, with experimetal data by Holden.[16] The compression creates an oblique shock, which induces a large increase in heat-transfer to the cooled wall. Given flow conditions are $M_\infty=8.03$, $U_\infty/\nu=5.35\times10^7$/m, $T_\infty=50.3$ K, and $T_w/T_\infty=5.89$. The experimental data indicate laminar-to-turbulent flow transition approximately between $x=12.7$ and 30.5 cm. The computation was carried out on a 200×50 grid, with at least five cells inside the viscous sublayer and with $y^+\le1$ at the first centroids away from the wall.

Figure 1 shows the curved ramp geometry and Fig. 2 the computational mesh. Figure 3 is a Mach contour plot, showing the oblique shock. Figure 4 is a comparison of heat-transfer predictions by the R_t, the linear (base) k–ϵ, and the cubic model with the experimental data. All calculations used a 1% freestream turbulence level and a length scale of 0.127 mm at the inflow boundary, located upstream of the ramp leading-edge. Each turbulence model predicted its own transition location and extent. The figure clearly indicates the advantage of the cubic model over the linear ones in predicting the flow transition region. This stems to some extent from Reynolds-stress anisotropy but mainly from the dependence of C_μ^* on mean strain and vorticity [see Eq. (4)]. This mechanism delays turbulence development in regions of high strain, found in developing boundary

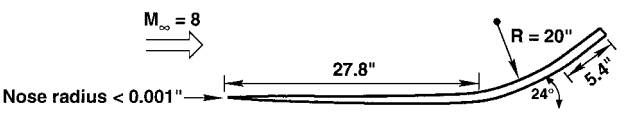

Fig. 1 Mach 8 ramp: geometrical details.

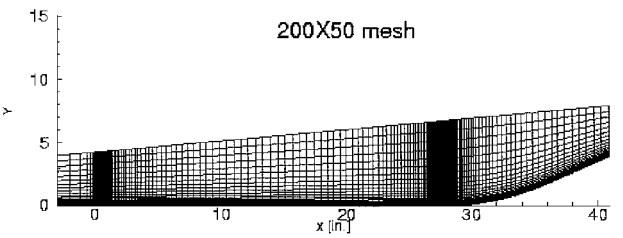

Fig. 2 Mach 8 ramp: computational mesh.

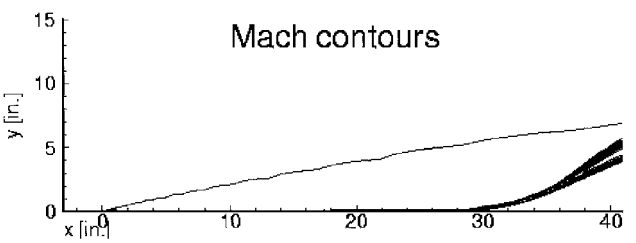

Fig. 3 Mach 8 ramp: Mach contours.

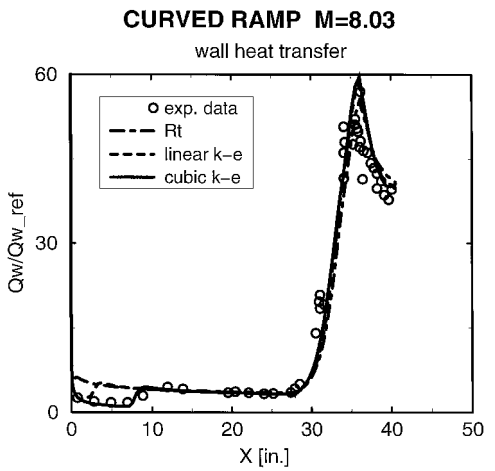

Fig. 4 Mach 8 ramp: effect of model on heat-transfer prediction.

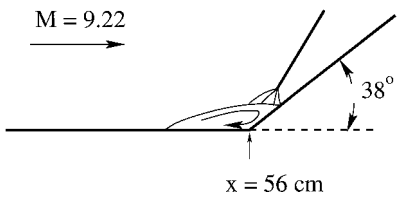

Fig. 5 Mach 9 ramp: geometry and flow features.

layers such as in leading-edge regions. This delay enables prediction of the laminar and transitional flow regions observed in this example. All models predict the heat-transfer peak correctly, however, in this nonseparating flow case.

B. Hypersonic Flow Case 2

This case is a two-dimensional Mach 9 flow over a 38-deg cooled ramp, with experimental data reported in Ref. 5. An oblique shock, impinging on the boundary-layer downstream of the ramp corner, induces flow detachment, with subsequent reattachment onto the ramp surface, where a large heat-transfer peak occurs. Figure 5 shows the geometry and main flow features. The flow conditions are as follows: $M_\infty = 9.22$, $Re_\infty = 0.47 \times 10^6$/cm, total temperature $T_0 = 1070$ K, $T_\infty = 64.5$ K, and wall temperature $T_w = 295$ K. Three single-equation turbulence closures were used to compute this flow: the R_t model, the S–A model, and Menter's model. The cubic k–ϵ closure was also tested. In lieu of adequate information about the experimental inflow conditions, a compressibility-corrected equilibrium 1-mm-thick turbulent boundary-layer (wake strength parameter $\Pi = 0.55$) was imposed at the inflow, together with the following profiles for k, ϵ, and R:

$$k = \left(\kappa^2 \Big/ C_\mu^{\frac{1}{2}}\right)\left[y\left(\frac{\mathrm{d}U}{\mathrm{d}y}\right)\right]^2 \qquad y^+ \le 11 \tag{21}$$

$$k = \max\left\{k_\infty, \left(\kappa^2 \Big/ C_\mu^{\frac{1}{2}}\right)\left[y\left(\frac{\mathrm{d}U}{\mathrm{d}y}\right)\right]^2\right\} \qquad y^+ > 11 \tag{22}$$

$$\epsilon = \frac{2A_\epsilon k^{\frac{3}{2}}}{y\left(1 - e^{-A_\epsilon \phi y^{+2}}\right)} \tag{23}$$

$$R = C_\mu k^2 / \epsilon \tag{24}$$

where $C_\mu = 0.09$, $A_\epsilon = C_\mu^{3/4}/(2\kappa)$, $\phi = 0.166$, and k_∞ was set to $8 \times 10^{-7} U_\infty^2$. In the preceding, $y^+ = y\rho u_\tau/\mu$, and the friction velocity $u_\tau = (\tau/\rho)_w^{1/2}$. This comprises a plausible and consistent set of inflow profiles; however, calculations with a slightly thicker boundary-layer as well as without a boundary-layer yielded very little change in the final results because of the limited upstream influence of the strong interaction region in this hypersonic flow case.

The computation was performed on a 250×200 grid with at least 20 cells inside the viscous sublayer and with the first centroidal locations away from the wall being at $y^+ \approx 0.1$. The grid was also clustered in the x direction, centered at the ramp corner. A 200×150 grid was also used to ascertain grid independence of the reported fine mesh results.

Figure 6 shows wall pressure and Fig. 7 heat-transfer distributions as predicted by the four models. Comparison with the experimental

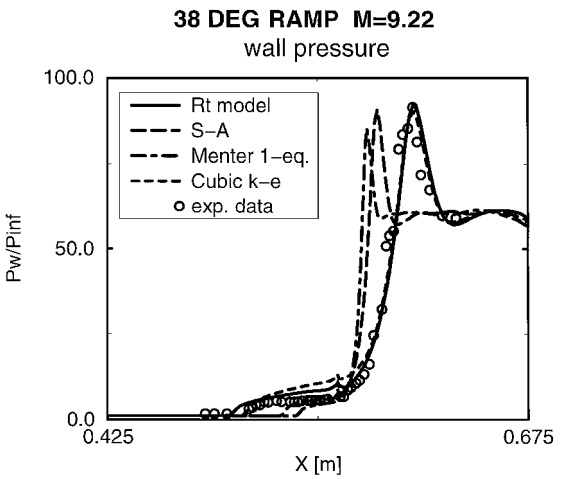

Fig. 6 Mach 9 ramp: wall pressure distribution.

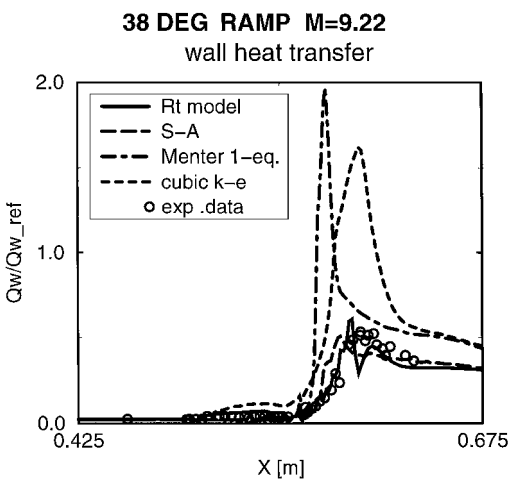

Fig. 7 Mach 9 ramp: heat-transfer distribution.

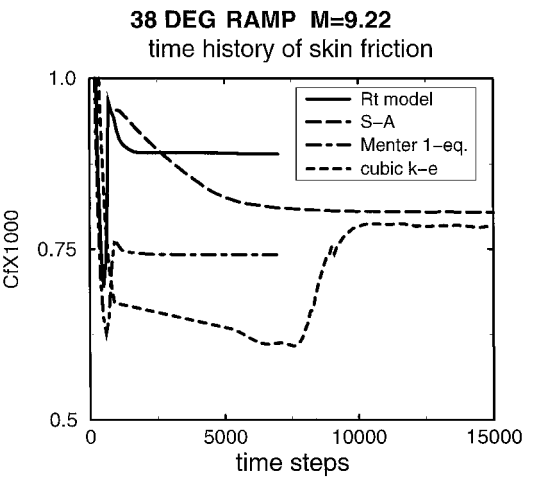

Fig. 8 Mach 9 ramp: convergence history.

data for both pressure and heat-transfer indicates that the one-equation R_t model yields the best overall prediction. It captures the extent of the flow separation region and also correctly predicts the shock location and the peak pressure level. The S–A model predicts less than half the size of the experimentally observed separation bubble, whereas Menter's model predicts an even smaller reversed flow; hence, both closures predict the shock too far upstream. The heat-transfer is, again, best predicted by the R_t closure, whereas the S–A model prediction is somewhat inferior. Menter's model yields a peak heat-transfer some four times the observed level, and the cubic model's performance is only slightly better, albeit the peak location is better predicted because of correct capturing of the separation bubble. The fact that the cubic model captures the pressure distribution almost as well as the R_t model does while its predicted heat-transfer is too high suggests that in separated flow regions with simultaneously low mean-flow kinetic energy (and therefore low strain magnitude) and high temperature gradients, overpredicted levels of turbulence length scale can lead to rather small errors in the turbulent shear stress while leading to a large overprediction of the turbulent heat fluxes. Figure 8 is a convergence history plot, based on skin friction, showing that the R_t and Menter's closure convergence rates are much better than those of the S–A and cubic model in this case.

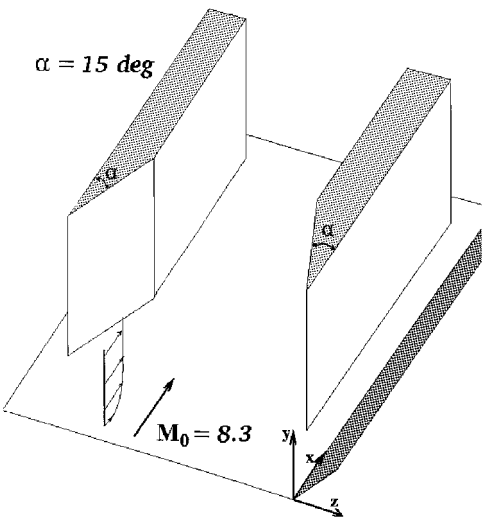

Fig. 9 Mach 8 inlet: sketch of geometry.

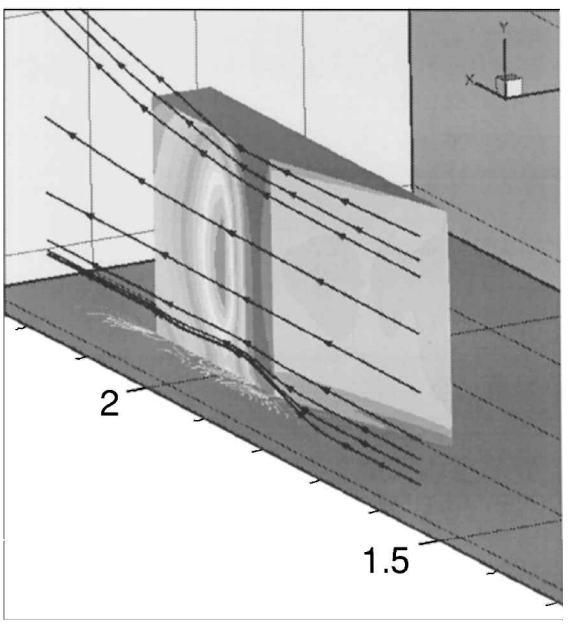

Fig. 10 Mach 8 inlet: flow features in wedge region.

The R_t model's superior performance stems from its derivation[2]: the near-wall formulation, particularly the function f_3, was obtained from asymptotic arguments, and all model constants, as well as the function f_μ, were derived to comply with limit arguments such as the logarithmic overlap layer, flow at duct center, flow with high pressure gradient and other unit cases. Menter's closure, on the other hand, was derived from the standard k–ϵ model, except for replacement of the relation $-|\widetilde{u_i u_j}| = a_1 k(P_k/\epsilon)^{1/2}$ with Bradshaw's hypothesis $-|\widetilde{u_i u_j}| = a_1 k$. However, the distinction between these formulations diminishes as a wall is approached because $k \sim y^2$; hence this closure's similarity to a k–ϵ model in its near-wall behavior.

C. Hypersonic Flow Case 3

Kussoy et al.[17] performed extensive experimental measurements on a Mach 8.3 flow in a wedge inlet configuration. To predict this complex three-dimensional flowfield, involving crossing shock/boundary-layer interactions, the flow solver was used on a mesh consisting of approximately 250,000 cells. Centroidal locations adjacent to walls were at $y^+ \approx 60$, and a wall function that accounts for compressibility and heat-transfer effects was employed. A solution to the wall would have entailed a considerably larger grid, deviating from current engineering practice. The R_t model was employed here on the strength of its performance in the Mach 9 case. For comparison, the cubic k–ϵ model was also used to predict this flow.

Figure 9 is a sketch of the topology. Figure 10 is an overview of the flow in the region of the wedges, showing pressure contours on one wedge surface and streamlines. The observation is made that the flow in the midregion of the wedge maintains an approximately two-dimensional flavor. The high-pressure region downstream of the shoulder is caused by crossing shock impingement from the other wedge. The streamlines at the wall/wedge junction clearly show streamwise separation caused by the adverse pressure gradient downstream of the wedge shoulder. Flow spillage at the top of the wedge, because of the cross-stream pressure gradient, is also observed.

Figure 11 compares R_t model prediction and data of surface pressure contours between the wedges, showing very good agreement. Lastly, Fig. 12 compares predicted wall pressure and heat-transfer,

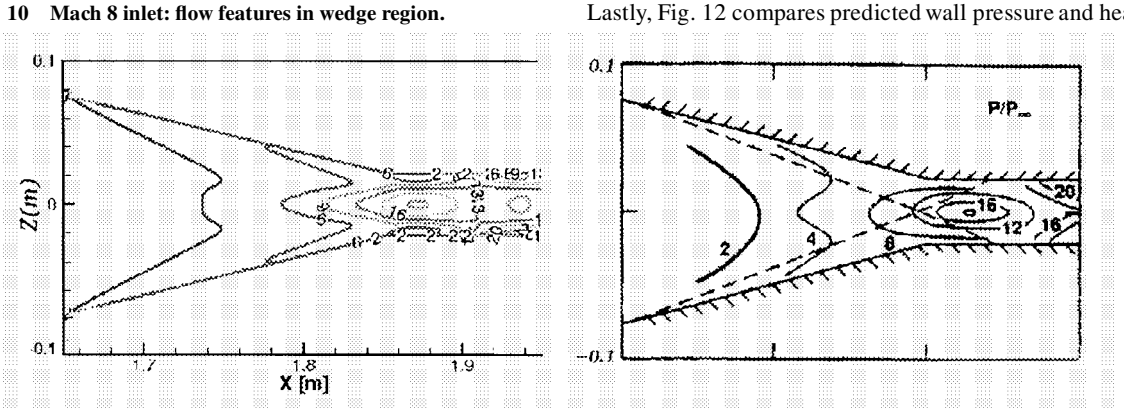

Fig. 11 Mach 8 inlet: surface pressure contours between the wedges—*L*, prediction; *R*, exp. data.

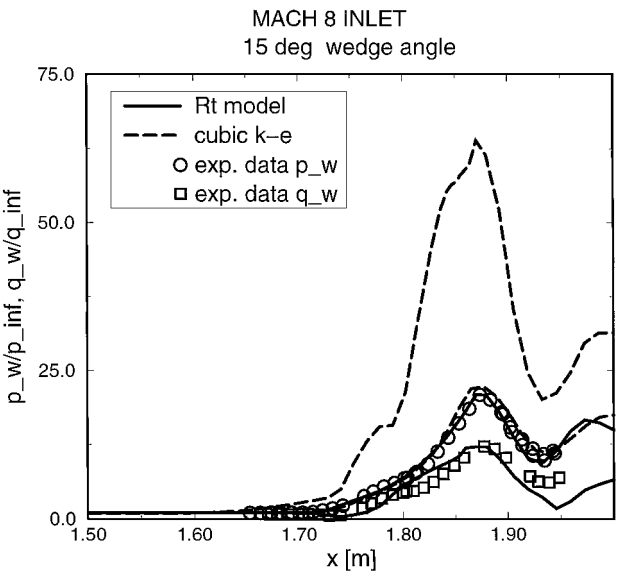

Fig. 12 Mach 8 inlet: pressure and heat-transfer profiles in symmetry plane.

along the symmetry line, with corresponding measurements. As in the Mach 9 case, the R_t model yields very good agreement with both pressure and heat-transfer data. The cubic k–ϵ closure exhibits the same trend observed in the preceding case: good pressure prediction and gross overprediction of heat-transfer. The near-wall inadequacy of the ϵ equation under strong nonequilibrium conditions evidently overwhelms the advantages of this nonlinear model, in terms of its otherwise superior physics, when it comes to heat-transfer prediction.

V. Conclusions

The CFD++ flow solver, in conjunction with the linear single-equation R_t model and a cubic k–ϵ turbulence closure, was used to predict three hypersonic flow cases. Comparisons with experimental data indicate that the code is able to predict these flows with high fidelity. Both closures performed well in predicting pressure distributions. Whereas the cubic model showed much promise in bypass transition prediction, the linear R_t model excelled in predicting heat-transfer levels, which are of prime importance in hypersonic flight vehicle design. The excessive levels of heat-transfer predicted by the cubic model suggest that in separated flow regions with simultaneously low mean-flow kinetic energy (and therefore low strain magnitude) and high temperature gradients overpredicted levels of turbulence length scale can lead to rather small errors in the turbulent shear stress, while leading to a large overprediction of the turbulent heat fluxes. Comparisons were also made against Menter's and S–A's single-equation models, which did not perform as well as the simpler one-equation R_t model did. This leads to the conclusion that the latter is a good candidate for engineering prediction of hypersonic flow heat-transfer. Future work will attempt to improve the cubic model's performance in this respect.

References

[1]Launder, B. E., "On the Computation of Convective Heat Transfer in Complex Turbulent Flows," *Journal of Heat Transfer*, Vol. 110, 1988, pp. 1112–1128.

[2]Goldberg, U., "A Topology-Free Single-Equation Turbulence Model," *Computer Methods in Applied Mechanics and Engineering* (submitted for publication).

[3]Spalart, P. R., and Allmaras, S. R., "A One-Equation Turbulence Model for Aerodynamic Flows," AIAA Paper 92-0439, Jan. 1992.

[4]Menter, F. R., "Eddy Viscosity Transport Equations and Their Relation to the k-ϵ Model," *Journal of Fluids Engineering*, Vol. 119, No. 4, 1997, pp. 876–884.

[5]Coleman, G. T., and Stollery, J. L., "Heat Transfer from Hypersonic Turbulent Flow at a Wedge Compression Corner," *Journal of Fluid Mechanics*, Vol. 56, Pt. 4, 1972, pp. 741–752.

[6]Goldberg, U., Peroomian, O., Palaniswamy, S., and Chakravarthy, S., "Anisotropic k-ϵ Model for Adverse Pressure Gradient Flow," AIAA Paper 99-0152, Jan. 1999.

[7]Shih, T. H., Lumley, J. L., and Zhu, J., "A Realizable Reynolds Stress Algebraic Equation Model," NASA TM-105993, 1993.

[8]Lien, F. S., and Leschziner, M. A., "Low-Reynolds-Number Eddy-Viscosity Modelling Based on Non-Linear Stress-Strain/Vorticity Relations," *Engineering Turbulence Modelling and Experiments 3*, edited by W. Rodi and G. Bergeles, Elsevier, Amsterdam, 1996, pp. 91–100.

[9]Loyau, H., Batten, P., and Leschziner, M. A., "Modelling Shock/Boundary-Layer Interaction with Non-Linear Eddy-Viscosity Closures," *Flow, Turbulence, and Combustion*, Vol. 60, 1998, pp. 257–282.

[10]Goldberg, U., Peroomian, O., and Chakravarthy, S., "A Wall-Distance-Free k-ϵ Model with Enhanced Near-Wall Treatment," *Journal of Fluids Engineering*, Vol. 120, No. 3, 1998, pp. 457–462.

[11]Goldberg, U., and Peroomian, O., "Hypersonic Flow Heat Transfer Prediction with Wall-Distance-Free Turbulence Models," *Computational Methods and Experimental Measurements IX*, edited by G. M. Carlomagno and C. A. Brebbia (eds.), WIT Press, U.K., 1999, pp. 261–270.

[12]Chakravarthy, S., Peroomian, O., and Sekar, B., "Some Internal Flow Applications of a Unified-Grid CFD Methodology," AIAA Paper 96-2926, July 1996.

[13]Peroomian, O., Chakravarthy, S., and Goldberg, U., "A 'Grid-Transparent' Methodology for CFD," AIAA Paper 97-0724, Jan. 1997.

[14]Peroomian, O., Chakravarthy, S., Palaniswamy, S., and Goldberg, U., "Convergence Acceleration for Unified-Grid Formulation Using Preconditioned Implicit Relaxation," AIAA Paper 98-0116, Jan. 1998.

[15]Batten, P., Leschziner, M. A., and Goldberg, U. C., "Average-State Jacobians and Implicit Methods for Compressible Viscous and Turbulent Flows," *Journal of Computational Physics*, Vol. 137, 1997, pp. 38–78.

[16]Holden, M. S., "Turbulent Boundary Layer Development on Curved Compression Surfaces," Calspan Rept. 7724-1, 1992.

[17]Kussoy, M. I., Horstman, K. C., and Horstman, C. C., "Hypersonic Crossing Shock-Wave/Turbulent-Boundary-Layer Interactions," *AIAA Journal*, Vol. 31, No. 12, 1993, pp. 2197–2203.